



ALMA MATER STUDIORUM  
UNIVERSITÀ DI BOLOGNA

ARCHIVIO ISTITUZIONALE  
DELLA RICERCA

## Alma Mater Studiorum Università di Bologna Archivio istituzionale della ricerca

Resolving the thickness of peat deposits with contact-less electromagnetic methods: A case study in the Venice coastland

This is the final peer-reviewed author's accepted manuscript (postprint) of the following publication:

*Published Version:*

Boaga J., Viezzoli A., Cassiani G., Deidda G.P., Tosi L., Silvestri S. (2020). Resolving the thickness of peat deposits with contact-less electromagnetic methods: A case study in the Venice coastland. *SCIENCE OF THE TOTAL ENVIRONMENT*, 737, 1-11 [10.1016/j.scitotenv.2020.139361].

*Availability:*

This version is available at: <https://hdl.handle.net/11585/764668> since: 2020-07-07

*Published:*

DOI: <http://doi.org/10.1016/j.scitotenv.2020.139361>

*Terms of use:*

Some rights reserved. The terms and conditions for the reuse of this version of the manuscript are specified in the publishing policy. For all terms of use and more information see the publisher's website.

This item was downloaded from IRIS Università di Bologna (<https://cris.unibo.it/>).  
When citing, please refer to the published version.

(Article begins on next page)

This is the final peer-reviewed accepted manuscript of:

Boaga J.; Viezzoli A.; Cassiani G.; Deidda G. P.; Tosi L.; Silvestri S.: Resolving the thickness of peat deposits with contact-less electromagnetic methods: A case study in the Venice coastland. Science of the total environment 737. 1-11. DOI: 10.1016/j.scitotenv.2020.139361

The final published version is available online at:

<http://dx.doi.org/10.1016/j.scitotenv.2020.139361>

Rights / License:

The terms and conditions for the reuse of this version of the manuscript are specified in the publishing policy. For all terms of use and more information see the publisher's website.

*This item was downloaded from IRIS Università di Bologna (<https://cris.unibo.it/>)*

***When citing, please refer to the published version.***

1 <https://doi.org/10.1016/j.scitotenv.2020.139361>

Formatted: Normal, Line spacing: single

2  
3 **Resolving the thickness of peat deposits with contact-less electromagnetic**  
4 **methods: a case study in the Venice coastland**

5  
6 Boaga J. <sup>(1)</sup>, Viezzoli A. <sup>(2)</sup>, Cassiani G. <sup>(1)</sup>, Deidda G.P. <sup>(3)</sup>, Tosi L. <sup>(4)</sup>, Silvestri S. <sup>(5)\*</sup>

7  
8 <sup>(1)</sup> Dept. of Geosciences, University of Padova, Padova, Italy

9 <sup>(2)</sup> Aarhus Geophysics ApS, Aarhus, Denmark

10 <sup>(3)</sup> Dept. of Civil and Environmental Engineering and Architecture, University of  
11 Cagliari, Cagliari, Italy

12 <sup>(4)</sup> Institute of Geosciences and Earth Resources, National Research Council, Via G.  
13 Gradenigo, 6 - 35131 Padova, Italy, luigi.tosi@igg.cnr.it

14 <sup>(5)</sup> Dept. of Biological, Geological and Environmental Sciences, University of Bologna,  
15 Ravenna, Italy

16 \* corresponding author

17  
18 **Abstract**

19 Peat soils are typical deposits characterizing wetlands and reclaimed farmlands. They  
20 are important carbon reservoirs and when degraded (e.g., erosive processes, fires,  
21 draining and plowing) massive carbon dioxide volumes are released. This leads to  
22 increase greenhouse effect and induce serious land subsidence. Thus, mapping the  
23 volume of peat deposits is crucial in order to estimate the carbon mass and the potential  
24 release of carbon dioxide and consequent loss in soil elevation. Despite the importance  
25 of such estimations, forecasting and quantifying the peat thickness is still a challenge.

26 Direct sediment coring provides local information that are difficult to extend to large  
27 territories. ~~Indirect geophysical methods are unable to resolve lithological contrasts in~~  
28 ~~the presence of saltwater contamination in coastal areas. Indirect geophysical methods~~  
29 ~~are often vanished by the presence of saltwater contamination in coastal areas.~~ In this  
30 work, we show the results obtained using two contact-less electromagnetic methods for  
31 the characterization of peat deposits in a peatland site of the Venice coastland, Italy.  
32 Specifically, a multi-frequency portable instrument (FDEM) and an airborne time-  
33 domain electromagnetic one (AEM) were used to collect data over a former wetland  
34 then reclaimed for agricultural purposes. Additional electrical resistivity tomography  
35 (ERT) data, ~~which are~~ known for their very high and relatively low vertical resolution  
36 respectively, are used together with sediment core data to assess the effectiveness and  
37 accuracy of the contact-less methods. Results show that both FDEM and AEM are very  
38 effective in detecting the presence of the peat layer, despite its low thickness (< 2 m)  
39 and the high electro-conductive subsoil because of saltwater contamination. However,  
40 the AEM method overestimated the peat thickness while the FDEM could accurately  
41 resolve the peat thickness even where the layer was thinner than 1 m. When compared  
42 to the electrical features extracted from the ERT, discrepancies are on average lower  
43 than 30-%; when compared to the borehole data, discrepancies are on average slightly  
44 higher than 6-%.

**Commented [DSSP1]:** Line 25: Suggest rephrasing the sentence beginning in this line. The verb "vanish" is poor English usage in this context. Try either of these sentences: "Indirect geophysical methods do not work well in the presence of saltwater contamination in coastal areas." OR "Indirect geophysical methods are unable to resolve lithological contrasts in the presence of saltwater contamination in coastal areas."

## 46 1. Introduction

47 Peatlands are important carbon pools and, if degraded, they release large amounts of  
48 carbon dioxide and other greenhouse gasses (Page et al., 2002; Turetsky et al., 2015).  
49 The organic carbon stored belowground is preserved by wet or moist soil conditions.

50 Once the soil is drained, as for example during prolonged droughts or for man-induced  
51 processes such as land reclamation, aerobic microorganisms decompose quickly the  
52 organic matter, releasing carbon dioxide and other gasses (e.g., Hooijer et al., 2012;  
53 Fenner and Freeman, 2011). The decomposition of organic matter also induces one of  
54 the most severe mechanisms of land subsidence, i.e. the geochemical subsidence  
55 (Zanello et al., 2011), which may cause meters of loss in ground elevation in a few  
56 decades.

57 At the global scale, the large majority of terrestrial carbon is stored in soils. It is  
58 estimated that vegetation stores about 500 Pg of carbon (considering both aboveground  
59 and belowground phytomass) while soils store between 1500 Pg (Scherlemann et al.,  
60 2014) and 2500 Pg (Batjes, 2014; Jansson et al., 2010) of carbon, and ~ 30% of it is  
61 stored in peatlands (Scherlemann et al., 2014; Bourgeau-Chavez et al., 2018). Peat  
62 degradation has been proven to contribute an enormous amount of greenhouse gasses  
63 to the atmosphere every year. The estimate of the global emission of CO<sub>2eq</sub> due to  
64 peatland drainage is very uncertain, and varies between 0.9 and 1.3 Gt CO<sub>2eq</sub>/yr  
65 (Joosten, 2010; FAOSTAT, 2013). This picture is even more alarming if we consider  
66 that the numerous fires that occur in forested wetland systems, especially in tropical  
67 areas, increase the amount of greenhouse gasses released every year (Turetsky et al.,  
68 2015; Ballhorn et al., 2009). In addition to the problems related to CO<sub>2eq</sub> emissions, the  
69 continuous conversion of tropical peatlands to agriculture and the hydraulic drainage  
70 of low-lying areas have resulted in widespread land subsidence creating great concern  
71 especially in coastal areas (e.g., Van Asselen et al., 2018).

72 Considering that the potential of releasing carbon dioxide and of peatland subsidence  
73 depends on the mass availability of the organic matter in the soil, the quantification of  
74 the peat extent over vast territories is a very relevant challenge. **Therefore, it is**

75 becoming urgent to develop methodologies that allow an accurate and fast mapping of  
76 soil organic carbon, with particular interest for wetlands and peatlands.

77 The most common and widely used method for peat deposit quantification and  
78 characterization relies on shallow borehole information and ground-based surveys  
79 using geophysical methods. In order to be effective at the regional scale and given the  
80 extent and thickness variability of peat, a method based on field measurements needs a  
81 large database of high-density distributed field observations, which are essential in  
82 order to correctly define the covariance model necessary to interpolate/extrapolate the  
83 point measurements (Keaney et al., 2013) and minimize spatial aliasing. In the  
84 literature, there are examples of studies reporting the collection of a large number of  
85 peat thickness measurements performed in the field using push probes (Parsekian et al.,  
86 2012; Householder et al., 2012; Holden and Connolly, 2011). However, even though  
87 the use of push probes is a relatively fast method and may provide large databases, it  
88 has been shown that the accuracy reached using exclusively soil probes is limited,  
89 leading to an average error of depth estimation as high as 35% (Parry et al., 2014). Soil  
90 coring guarantees much higher accuracies in measuring the peat thickness locally,  
91 however it is extremely time consuming especially in wetland environments and does  
92 not allow the collection of large enough databases. In order to overcome these issues,  
93 various traditional ground-based geophysical techniques have been successfully  
94 applied for peat characterization. For example, ground penetrating radar (GPR) (e.g.,  
95 Comas et al. 2017; Comas et al., 2015; Parsekian et al., 2012; Slater and Reeve, 2002),  
96 electrical tomography (ERT) (e.g., Walter et al. 2019; Comas et al., 2015; Elijah et al.,  
97 2012; Boon et al., 2008;) and induced polarization (IP) methods (e.g., Comas and Slater,  
98 2004; Slater and Reeve, 2002) together with complementary borehole data.

Commented [DSSP2]: Line 95: change complement to complementary

99 Nevertheless, the use of soil cores and traditional ground-based geophysical techniques  
100 are generally limited, being moist and wet soil conditions difficult accessible and the  
101 relatively local scale of the investigations obtainable. ~~Moreover, the presence of dense~~  
102 ~~vegetation cover peatlands are usually covered with very dense vegetation that~~  
103 ~~represents an additional challenge for traditional ground-based geophysics.~~

**Commented [DSSP3]:** Lines 98-99. Check English in the second phrase of this sentence

104 Recently, Silvestri et al. (2019a, 2019b) used airborne electro-magnetic (AEM) to  
105 identify peat layers over large territories in a Norwegian study site characterized by the  
106 presence of several bogs and in a large Indonesian peatland respectively. In both these  
107 frameworks, the AEM method proved to be highly effective to distinguish the electrical  
108 properties of the peat layer from that of the substrate, ~~allowing delineation of their~~

**Commented [DSSP4]:** Lines 106-107. Change the phrase "allowing to drawn their boundary" to "allowing delineation of their boundaries."

109 ~~boundaries~~ ~~allowing to drawn their boundary~~. Higher vertical resolution is obtained with  
110 the presence of conductive substrate while the uncertainty increases for resistive  
111 substrates. However, through a sensitivity analysis, Silvestri et al. (2019a, 2019b) show  
112 that the accuracy reached using exclusively the AEM method is generally not sufficient  
113 to resolve thin peat layers, roughly 1-1.5 m thick. Therefore, an alternative approach is  
114 needed to investigate thin peat layers over large areas.

115 In this paper, we present the results obtained by testing for the first time a contact-less  
116 frequency domain electromagnetic method (FDEM) for resolving the peat thickness.  
117 The main advantage of this method is that it is suitable for meso-scale peatland  
118 characterization of difficult-to-access areas, but also tries to overcome the limited  
119 vertical resolution that affects the AEM technology. A comparison of the vertical  
120 accuracies obtained with both AEM and FDEM methods is also performed and  
121 discussed.

122 The pilot area selected for this study is a low-lying peatland used for farmland, located  
123 between the Po river delta and the Venice Lagoon, Italy. Most of the farmland is derived

124 from the hydraulic reclamations of ancient wetlands and lagoons, which started at the  
125 beginning of the last century, and today lies below mean sea level.

126 Information on the peat thickness is very limited as it is available only from sediment  
127 cores, which provide local details. In general, the peat layer thickness is lower than 2  
128 m because the original uppermost layers were oxidized during the last century due to  
129 the hydraulic drainage and agricultural activities, which induced geochemical  
130 subsidence (Tosi et al., 2009). Tosi et al. (2000) computed rates of up to 3-4 cm/yr of  
131 loss in elevation during the last century. Such large historical rates come from a number  
132 of concomitant causes of land subsidence that included (i) the groundwater pumping  
133 occurred in the 1950-1960 period (contributing about 1-1.5 m to the total subsidence),  
134 (ii) exploitation of gas-bearing waters (from late 1940s to late 1960s), (iii) the common  
135 practice of burning grass and vegetation that grew along the banks of the hydraulic  
136 drainage network causing the peat to burn. In addition, the maintenance of a very low  
137 water table (by pumping stations) during rainy periods in order to avoid sudden floods  
138 increased for decades the oxidation of organic soils and therefore facilitated the  
139 geochemical subsidence. Today, groundwater exploitation and the agriculture practice  
140 of burning vegetation are no longer used, and the beginning of 2000's the hydraulic  
141 reclamation drainage management allows to keep the water table higher than in the past,  
142 significantly reducing land subsidence rates. Even though the rates are considerably  
143 smaller than in the past, it has been shown that the land is still subsiding at a rate of 3-  
144 15 mm/yr, calculated for the recent years (Zanello et al., 2011) releasing in the  
145 atmosphere  $9.2 \pm 5.5 \text{ kg CO}_2 \text{ m}^{-2} \text{ yr}^{-2}$  (Camporese et al., 2008).

146 The selected case study is particularly challenging from the geophysical point of view  
147 because thin peat deposits are hard to distinguish from the underlying conductive  
148 substrate that consists of clay and silty-clay layers, often salinized by saltwater



149 intrusion. In fact, the organic matter present in peat soils has similar electrical properties  
150 to conductive substrates (Silvestri et al. 2019b), producing a modest resistivity contrast  
151 that makes it problematic to detect the discontinuity at the bottom of the peat. Despite  
152 the challenges, our findings show that contact-less geophysical methods as FDEM and  
153 AEM can successfully detect the presence of peat deposits. While AEM tends to  
154 overestimate the peat thickness of thin peat deposits, FDEM can accurately resolve also  
155 very thin peat layers.

156

## 157 2. Study site

158 The study site is the Zennare basin, which is part of a larger low-lying area located  
159 between the southern margin of the Venice Lagoon and the northern Po river delta  
160 (Italy) (Fig. 1). The area is characterized by Holocene deposits with a variety of  
161 geomorphic features, as for example ancient fluvial ridges, paleo-river beds and paleo-  
162 coastlines (Rizzetto et al. 2003). The basin is currently below the mean sea level and it  
163 mostly consists of high value agricultural land established after the hydraulic  
164 reclamation of pre-existing lagoons and wetland areas that started in the Veneto Region  
165 in 1892. Today, the basin is surrounded by levees; ditches regulate the surface waters  
166 and pumping stations stabilize the water table at about 0.5 m below the land surface,  
167 discharging the drainage water into the Venice Lagoon or the Adriatic Sea.

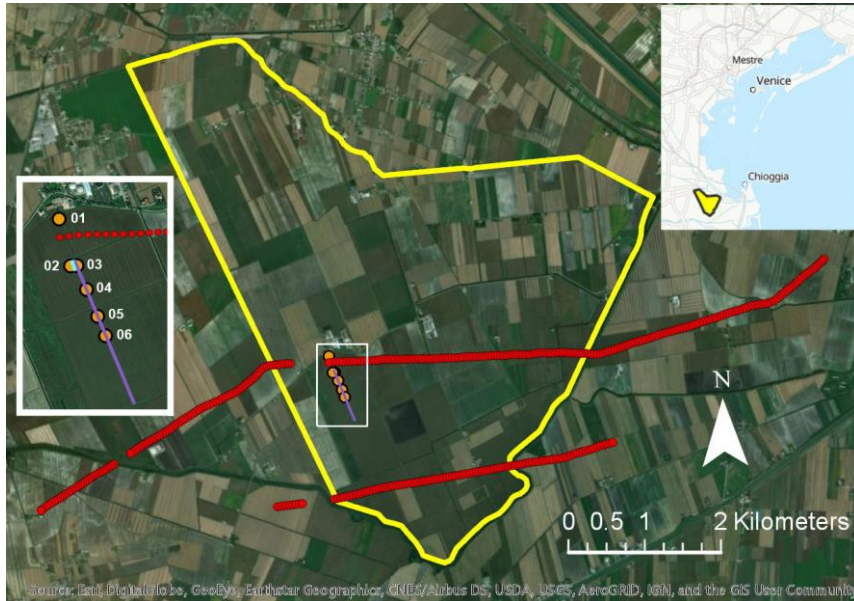
168 Over the past century, oxidation of the organic soil fraction in response to drainage for  
169 farming provoked the degradation of the shallow peat deposits leading to serious land  
170 subsidence rates, often one order of magnitude higher than the natural ones caused by  
171 sediment compaction and tectonic movements (e.g., Tosi et al., 2009; Tosi et al., 2010;  
172 Tosi et al., 2016). Evidence of peat-oxidation land settlements, e.g., the protrusion of

173 old hydraulic structures founded on the stiff clays and sands underlying the outcropping  
174 peat, and ground- and satellites-based monitoring data allowed to quantify up to 2-3  
175 cm/yr of loss in surface elevation (Tosi et al., 2000; Gambolati et al., 2005; Tosi et al.,  
176 2016). Consequently, the basin today lays between 2 and 4 m below the mean sea level  
177 (Rizzetto et al., 2003; Gasparetto-Stori et al., 2012). Ridges corresponding to sand filled  
178 paleochannel systems not affected by geochemical subsidence due to oxidation of the  
179 organic matter show higher elevations than the nearby peat soils.

180 The outcropping peat deposits extend for most of the basin (e.g., Nicoletti et al., 2003).  
181 The large majority of the shallow peats originally present in the area have been  
182 degraded due to geochemical subsidence as consequence of the oxidation of the organic  
183 soil. Currently the thickness of the peat layer is almost half of the original one and varies  
184 between less than 1 m to a maximum of 2 m across the basin (Rizzetto et al., 2003).

185 The shallow sequence is constituted by a c.a. 50 cm of ploughed and oxidized soil at  
186 the top and a peat with well-preserved fibers in growing position at the bottom. At the  
187 base, there is a transition layer of clayey peat gradually passing to clay with spread  
188 vegetable remains (Gatti et al., 2001). Peats derive from the accumulation of reeds  
189 (*Phragmites australis*) living in wetlands before the reclamation (Gatti et al., 2001).

190 Soil salt contamination partly affects the Zennare Basin (e.g., Rizzetto et al., 2003). The  
191 saltwater intrusion is favored by the land elevation that is well below the mean sea level  
192 but also by the presence of sandy paleo-channels crossing the farmland with main  
193 direction from inland to the lagoon boundary.



194  
 195 **Fig. 1 – The Zennare basin is outlined in yellow.** The map inset on the top-right shows  
 196 the location of the basin with respect to the Venice lagoon (Italy). The red lines  
 197 correspond to the AEM flight lines. The white rectangle shows the location of the  
 198 ground-based field surveys and is magnified within the inset to the left of the figure,  
 199 where the orange dots indicate the shallow boreholes, the purple line corresponds to the  
 200 FDEM transect and the short light-blue line shows the location of the ERT transect.

201

### 202 3. Methods

203 The dataset collected and analyzed in this study includes (see Fig. 1 for locations): (i)  
 204 frequency domain ground-based electro-magnetic (FDEM) data, (ii) ERT data along  
 205 **the initial portion of the FDEM transect, (iii) an aerial AEM survey along 2 flight-lines,**  
 206 **and (iv) borehole data collected along the FDEM transect, in order to get lithological**  
 207 **information and peat layer thickness.**

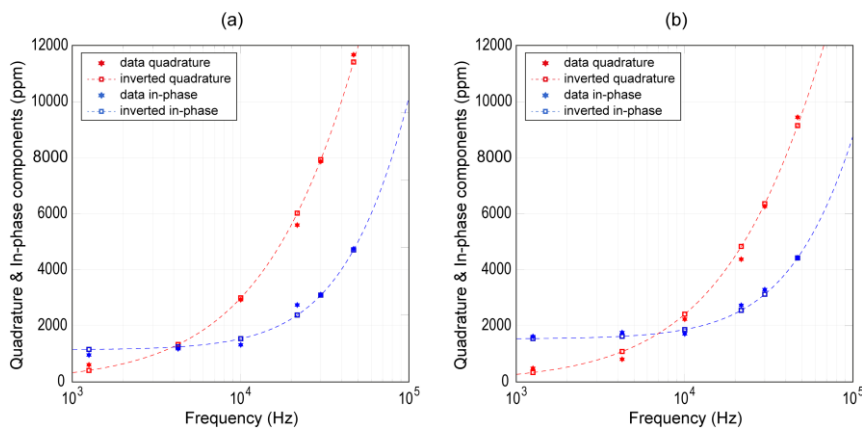
208 With reference to other studies carried out in the Venice coastland (e.g., Carbognin et  
209 al., 2003; de Franco et al., 2009; Viezzoli et al., 2009; Teatini et al., 2011; Da Lio et al.,  
210 2015), electrical resistivity  $<5 \Omega \cdot m$  and  $>10 \Omega \cdot m$  are respectively the upper and lower  
211 values for saltwater and freshwater, in terms of the electro-lithological units.

### 212 3.1 Frequency Domain Electro-Magnetic (FDEM) survey

213 The FDEM survey was performed in Fall 2018 using a GEM-2 probe manufactured by  
214 Geophex (www.geophex.com). The FDEM system is a multi-frequency probe, capable  
215 of investigating electrical properties of several depths at the same time (e.g., Boaga,  
216 2017, 2018; Deidda et al., 2014). The probe has one transmitter and one receiver coils,  
217 with a fixed separation of 1.66 m, and a multifrequency operation in the bandwidth 30  
218 Hz - 93 kHz. GEM-2 can be used as a conductivity meter for depth sounding when it  
219 operates in a range of moderate induction number (McNeill, 1980), for which the  
220 responses are strong and frequency dependent (Huang and Won, 2003). To meet this  
221 requirement, as the area is underlined by fairly conductive sediments, we used six  
222 frequencies ( $f_1 = 1,250$  Hz,  $f_2 = 4,250$  Hz,  $f_3 = 10,025$  Hz,  $f_4 = 21,750$  Hz,  $f_5 = 30,025$   
223 Hz, and  $f_6 = 47,025$  Hz) in order to span the range of induction numbers between 0.1166  
224 and 0.7152, and assuming the worst condition of a nonmagnetic half-space with a  
225 conductivity equal to 1 S/m.

226 The GEM-2 probe was carried by the operator along a 700 m NW-SE transect (see Fig.  
227 1 for location), at a constant height of about 1 m from the surface. The FDEM probe  
228 was connected to a Trimble GPS receiver to record the spatial coordinates for each  
229 measurement (with a total of about 12,000 points). Raw data were then processed  
230 focusing on the area where ERT data and control boreholes (03 and 04) are available  
231 (see section 3.3).

232 Prior to the inversion, data collected along the first 200 m of the transect were spatially  
 233 resampled at 1 m interval to set up a data set consisting of a series of 201 geometric  
 234 depth soundings with six complex (quadrature and in-phase components) GEM-2  
 235 responses. The complex response recorded at each sounding point was individually  
 236 inverted to infer the electrical conductivity depth profile using the FDEMtools (Deidda  
 237 et al., 2019), a free MATLAB software package implementing the numerical algorithms  
 238 mainly discussed by Deidda et al. (2014, 2017).  
 239 A layered starting model, with the layer conductivities based on ERT results, was used  
 240 for all one-dimensional inversions. In addition, to best fit the in-phase data at lower  
 241 frequencies, the relative magnetic permeability was set at 0.995 (i.e., a magnetic  
 242 susceptibility of  $-0.005$ , a value representative of diamagnetic materials) in the top 1  
 243 m portion of the model. As shown in Deidda et al. (2020), in this case too the inversion  
 244 of the complex signals has provided better results than the inversion of the quadrature  
 245 (imaginary part) component of the secondary to primary magnetic field ratio alone,  
 246 reaching root mean squared errors lower than 10%. Fig. 2 shows two examples of data  
 247 fitting, which relate to electromagnetic soundings co-located with boreholes 03 (Fig.  
 248 2a) and 04 (Fig. 2b).



250 Fig. 2 – Quadrature (red) and in-phase (blue) components of the secondary magnetic  
251 field response (ppm of the primary) as a function of frequency for electromagnetic  
252 soundings at 24 m (a) and 142 m (b) from the beginning of the FDEM transect. Stars  
253 and squares represent measured and predicted data, respectively.

254

### 255 **3.2 Electrical Resistivity Tomography (ERT) data**

256 Along the first portion of the selected transect we also acquired an ERT transect with  
257 the purpose of calibrating and comparing the resulting electrical resistivity values with  
258 those obtained using the FDEM method. We adopted a 48 electrodes setup with 0.5 m  
259 electrode spacing, for a total ERT length of 23.5 m. This ensures a depth of  
260 investigation of about 5 m (1/4-1/5 of the ERT line length).

261 We used a dipole-dipole skip 0 configuration – i.e. with dipole lengths equal to the  
262 minimum electrode spacing - collecting both direct and reciprocal measurements, in  
263 order to control the quality of the raw data (e.g., Cassiani et al., 2006). Data were  
264 collected with a Iris Instrument Syscal Pro resistivity meter, and were then inverted  
265 using the R2 code (e.g., Binley, 2015). The collected dataset is of high quality, since  
266 the 96% of the data pass the reciprocals check using a 5% error threshold.

### 267 **3.3 Airborne Time Electro-Magnetic (AEM) data**

268 Airborne Time Electro-Magnetic (AEM) data were collected in **Fall 2013** in the context  
269 of the National Flagship Project RITMARE (Tosi et al., 2018). **The project aimed at**  
270 **providing** a step forward in the delineation of the continental and marine surface water–  
271 groundwater interactions and the mechanisms controlling the saltwater intrusion,  
272 overcoming the intrinsic constraints typical of ground-based surveys. **Within the**

273 RITMARE framework, the SkyTEM helicopter-deployed time domain electro-  
274 magnetic system was chosen as its dual moment provides a bandwidth (i.e. a penetration  
275 range) suitable for applications where both near-surface and deep information is  
276 important to refine the hydrogeologic model (e.g., Teatini et al., 2011; Sørensen &  
277 Auken, 2004). During the flight, current flows through a transmitter loop carried below  
278 the helicopter at an altitude of about 30 m, setting up a magnetic field. The eddy currents  
279 induced below the ground surface generate a secondary magnetic field, and a receiver  
280 coils on the frame detects its temporal variation. SkyTEM data have been recently  
281 proven very effective in characterizing peatlands in boreal and tropical areas (Silvestri  
282 et al. 2019a, 2019b).

283 The AEM data have been re-processed in order to attempt to maximize the accuracy for  
284 the detection of the near-surface soil layers. The data have then been inverted using two  
285 homogeneous starting models, with initial conductivity of 30  $\Omega\cdot\text{m}$  and 5  $\Omega\cdot\text{m}$ . For  
286 both cases, the inversion was performed using 40 and 5 layers.

### 287 **3.4 Shallow borehole data**

288 The field surveys were performed in Fall 2018 and Spring 2019. The thickness of the  
289 peat layer was measured at six locations localized using GPS (Tab. 1). The samples  
290 were retrieved using an auger peat corer with diameter of 2.5 cm and 50 cm length.

291 Mechanical extensions were used in order to reach the bottom of the peat layer and  
292 characterize the transition surface towards the sand below. A small sample of substrate  
293 was collected at each location in order to determine its characteristics.

294 Geological and hydrogeological data collected within previous research projects and  
295 available through the websites of Città Metropolitana Venezia

296 (<http://webgis.cittametropolitana.ve.it/geologia>) have also been used to support the  
297 validation and interpretation of the geophysical outcomes.

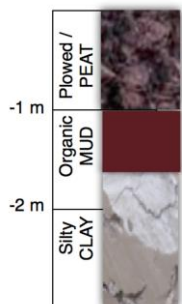
298

#### 299 4. Results

300 Tab. 1 summarizes the outcomes for all the boreholes and includes a sample lithology  
301 corresponding to borehole 01 (see Fig. 1 for location). All shallow boreholes show a  
302 similar lithology, which includes a layer of peat in the uppermost portion, with a  
303 transition zone characterized by mud mixed with peat and silty-clay underneath.

304 The thickness of the peat deposits is very thin and has a pronounced spatial variability  
305 ranging from 83 cm (borehole 06) to 210 cm (borehole 2) (Tab. 1), with an average  
306 value of 134 cm and standard deviation of 54 cm.

307 The analysis of other cores taken in the Zennare Basin (Gatti et al., 2001; Carbognin  
308 and Tosi, 2003; Città Metropolitana di Venezia) confirms the fairly homogenous  
309 lithology with variable thickness of the peat layer. Sands and silts are found only in  
310 correspondence of paleo-channels.



| Borehole ID | Easting coordinate | Northing coordinate | Peat thickness (cm) | Substrate                 |
|-------------|--------------------|---------------------|---------------------|---------------------------|
| 01          | 12.14083           | 45.17278            | 190                 | loamy-clay                |
| 02          | 12.14139           | 45.17084            | 210                 | silty-clay                |
| 03          | 12.14176           | 45.17084            | 130                 | silty-clay with fine sand |
| 04          | 12.14226           | 45.16984            | 95                  | silty-clay                |
| 05          | 12.14283           | 45.16873            | 98                  | silty-clay                |
| 06          | 12.14325           | 45.16791            | 83                  | silty-clay                |

311

312

313 Tab. 1 – Data corresponding to the boreholes and sample lithology found for borehole

314 01.

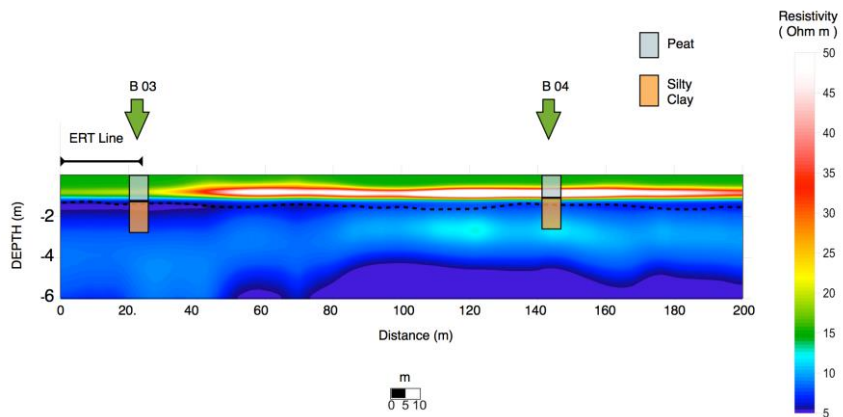


315

316 As explained in the Methods section, we inverted the multi-frequency FDEM data  
317 collected along a 200 m long transect overlapping the ERT line and the control borehole  
318 03 and 04.

319 The resulting one-dimensional models, with 60 layers to a depth of 6 m below the  
320 ground surface, are stitched together and plotted as a pseudo two-dimensional section  
321 in Fig. 3. The electrical resistivities vary gradually in the lateral direction, although they  
322 have been obtained by inverting data, sounding by sounding, without any lateral  
323 constraint. This is in agreement with the ERT evidence shown below in Fig.4.

324 Moreover, in agreement with the borehole information, the FDEM data substantially  
325 divide the Zennare subsoil in 2 layers: an upper resistive layer with about 1 m thickness  
326 lying on an electrically conductive subsurface. The first, with resistivities up to  $50 \Omega \cdot m$ ,  
327 represents the peat deposits, while the latter, with resistivities less than  $12 \Omega \cdot m$ , is  
328 representative of the silty/clayey – clayey saturated layers (similar values can be found  
329 e.g. in the fine sediments of the Venice lagoon - e.g. Boaga et al., 2014). In this very  
330 conductive environment, the peat deposits appear to be more resistive ( $>12 \Omega \cdot m$ ) in  
331 agreement with what already observed at other sites (Silvestri et al., 2019a, 2019b;  
332 Kowalczyk et al., 2017; Boon et al., 2008). These results confirm a substantial  
333 agreement with the information coming from the shallow boreholes, confirming that  
334 the average thickness of the peat layer in the study site is  $\sim 1.3$  m. Specifically,  
335 considering the  $12 \Omega \cdot m$  resistivity threshold as the bottom of the peat layer and  
336 averaging all the thickness values corresponding to such threshold along the transect,  
337 we obtain a mean peat thickness of 128 cm, with a difference of 6 cm with the average  
338 value calculated from boreholes in that zone.



339

340 Fig. 3 - Inverted electrical resistivity profile obtained from the FDEM multi-frequency

341 data. The dashed line indicates the 12  $\Omega \cdot m$  contour line as in Fig. 4. The location of the

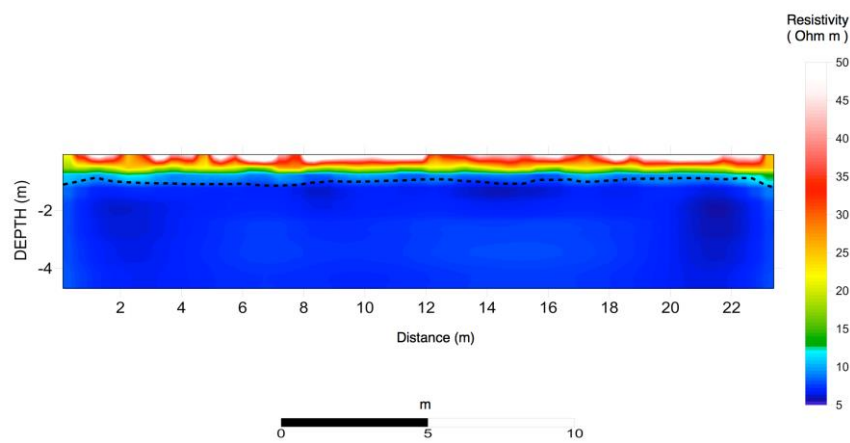
342 ERT line (Fig. 4) is marked to the left. Tab.1 borehole lithology is also presented.

343

344

345

346



347

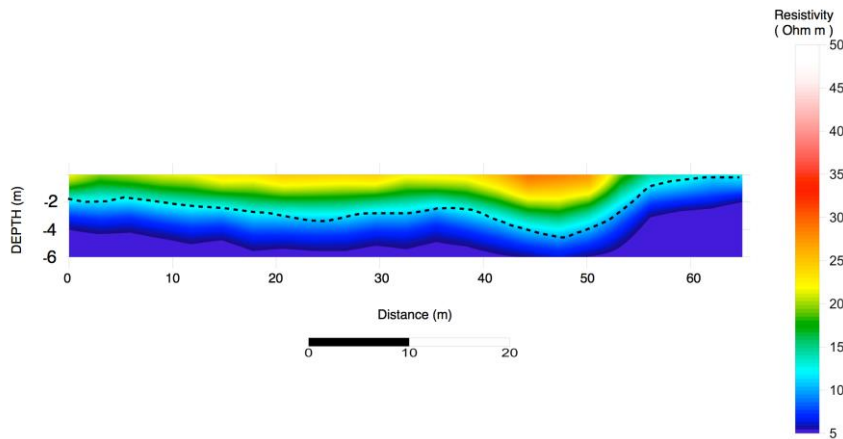
348 Fig. 4 - ERT inverted resistivity section (Fig.1 for location). The uppermost peat layer  
349 is more resistive than the underlying silty clay layer having a lower electrical resistivity  
350 ( $< 12 \Omega \cdot \text{m}$ ). The dashed line indicates the  $12 \Omega \cdot \text{m}$  contour line as in Fig. 3.

351

352 The resistivity values retrieved using the ERT profile are shown in Fig. 4 for  
353 comparison with the FDEM inversion in Fig. 3. The ERT and FDEM results agree to a  
354 very large extent: the shallow electrically resistive layer (values  $> 12 \Omega \cdot \text{m}$ ) lies on a  
355 conductive layer below. The contact between the two layers is at about 1 m depth, and  
356 this coincides with the transition between the peat and the underlying silty/clay layer  
357 (dashed line in Figs. 3-4), as detected by the direct borehole investigations. The ERT  
358 data confirm the continuity of the peat layer across the study site with no substantial  
359 lateral variations.

360 The results obtained from the inversion of the longest (northern) AEM flight line (see  
361 location in Fig. 1) are shown in Fig. 5. In this case 40 layers and initial conductivity of  
362  $30 \Omega \cdot \text{m}$  were used. Similar profiles were extracted for the second AEM flight line (the  
363 southern one) given the same initial conditions. Other inversions were performed in  
364 order to test the consistency of the method, and the results are shown in fig. A1 of the  
365 Appendix (i.e. four inversion setups are shown: a) 40 layers and starting with initial  
366 conductivity of  $30 \Omega \cdot \text{m}$ ; b) 40 layers and starting with initial conductivity of  $5 \Omega \cdot \text{m}$ ; c)  
367 5 layers and starting with initial conductivity of  $30 \Omega \cdot \text{m}$ ; d) 5 layers and starting with  
368 initial conductivity of  $5 \Omega \cdot \text{m}$ ). Note that the initial resistivity value in the inversion has  
369 small to no influence on the final resistivity model, indicating that the model quickly  
370 loses memory of the initial conditions, and that the inversion is robust. The similarity  
371 of the results obtained with the inversions performed using 40 layers and 5 layers tells  
372 us that the inversion consistently detects a more resistive surface layer over a

373 conductive substrate. This indicates that, despite the different resolution capabilities  
374 due to the remote sensing setup, the results obtained using the AEM method confirm  
375 the presence of an upper resistive layer corresponding to the peat deposit (Fig. 5).



376  
377 Fig. 5 – Extracted of the AEM results along line A falling within the white rectangle in  
378 Fig. 1. Here, like for ERT and FDEM results, the uppermost resistive layer ( $>12 \Omega \cdot m$  -  
379 peat) overlies the more conductive substrate ( $< 12 \Omega \cdot m$  – silty clay). The dashed line  
380 indicates the  $12 \Omega \cdot m$  contour line.

381  
382 Even though the AEM flight-line does not overlap with the ERT and FDEM transects  
383 and with the borehole investigations, we can conclude that AEM is in substantial  
384 agreement with the results obtained with the other methods. In fact, the AEM method  
385 can detect the presence of the peat layer, even though it is very thin, and the resistivity  
386 values detected by AEM are in good agreement with those obtained with ground based  
387 FDEM and ERT. As for the peat thickness, if we consider the  $12 \Omega \cdot m$  resistivity  
388 threshold as we did for the FDEM inverted data, we obtain for the AEM data an average  
389 peat thickness of 260 cm, which is considerably higher than the average value  
390 calculated for FDEM (128 cm) and from boreholes (134 cm). We can conclude that

18

391 AEM tends to overestimate the peat thickness and this is probably due to a low vertical  
392 resolution in a very-near-surface framework.

393

## 394 **5. Discussion**

395 Coastal wetlands are among the ecosystems that have mostly changed over the last  
396 century, especially those converted to agricultural lands by hydraulic reclamations. The  
397 soil rich in organic matter and peat layers makes farmlands highly productive, as in the  
398 case of the selected study site. However, the drainage systems necessary for keeping  
399 the water table level below the ground surface together with the plowing activities, are  
400 responsible of massive carbon dioxide release. This process likely increases greenhouse  
401 gasses and relative sea level rise because of the geochemical land subsidence triggered  
402 by the oxidation of organic matter.

403 Understanding how peatlands contribute to these processes requires detailed knowledge  
404 on the peat layer thickness. In general, the areal extent of the peatlands can be retrieved  
405 by satellite images (e.g., Nicoletti et al., 2003; Ballhorn et al., 2011; Draper et al., 2014;  
406 Jaenicke et al., 2008) while the assessment of their thickness over large areas is a  
407 challenge, especially where the peat layer is thinner than 1-2 m and saltwater  
408 contamination affect the shallow subsoil. In these environmental conditions, in fact,  
409 organic soil, peat and saturated clay are expected to have similar electrical properties.  
410 Peat is expected to have slightly higher resistivity with respect to the underlying clayey  
411 materials, with resistivity values for the peat in the order of 20-50  $\Omega \cdot m$  (compare e.g.  
412 with Kowalczyk et al., 2017). Ground-contact geophysical methods, such as ERT, have  
413 been extensively used in previous studies to resolve peat thickness and electrical  
414 characteristics (Boon et al., 2008; Comas et al., 2015; Elijah et al., 2012). Our  
19

415 experience confirms that ERT, applied to our study site, provides excellent results and  
416 high-resolution imaging, and is able to discern peat resistivity properties from the  
417 silty/clayey layers. However, when the peat layer is thin, ERT data must be collected  
418 with very small electrodes spacing in order to characterize the peat with high vertical  
419 resolution. In our case study, for example, we used a distance between electrodes of 0.5  
420 m, and a better resolution would require an even smaller spacing. This implies that if  
421 the targets are thin peat layers, and the area to be covered is large, field-work can  
422 quickly become overwhelming in terms of time and manpower. Thus, a demand for  
423 faster and still accurate subsoil investigation methods is pressing.

424 Contact-less methods, if properly applied, have the advantage of providing fast results  
425 for the characterization of large territories. Moreover, contact-less instruments can be  
426 easily carried for long distances, across difficult-to-access territories, permanently  
427 flooded or covered with dense vegetation. Our results show that such methods can be  
428 very effective in detecting the presence of peat layers, both from ground based and  
429 helicopter deployed sensors (i.e. FDEM and AEM method respectively). We show that,  
430 if compared to the results obtained with ERT at the Zennare site, the contact-less ground  
431 based FDEM technique and the remote airborne EM are both able to detect the presence  
432 of the peat layer patterns and estimate the same range of resistivity values for peat and  
433 subsoil. Our results show that, for conductive substrates, the peat presence can be  
434 detected using AEM even when the peat layer is very thin; however, we also show that  
435 AEM tends to overestimate the peat thickness. This result confirms the tendency of  
436 AEM to overestimating thin peat layers that was found by Silvestri et al. (2019b) in  
437 case of peats over conductive substrates in an Indonesian study site. On the contrary,  
438 FDEM shows a superior accuracy in resolving the peat thickness, even for very thin  
439 peat deposits. If we consider  $12 \Omega \cdot m$  as the threshold value that separates the peat layer

440 from the substrate, we have on average a difference of less than 10 cm between the  
441 average peat thickness resolved by the FDEM instrument along the transect and the  
442 average thickness measured through probing. Such difference increases to 130 cm for  
443 the AEM data. Even if we must notice that the AEM flight lines do not overlap with the  
444 FDEM/ERT transect, we speculate that the difference is mainly due to the low vertical  
445 resolution of the AEM and not to an actual variability of the peat layer thickness, which  
446 is highly unfeasible at this study site. Note that, had we performed a contemporary  
447 FDEM and AEM campaign over common transects, a joint inversion of ground-based  
448 and airborne EM data would be possible and may potentially improve the final accuracy  
449 of the retrievals.

450 These considerations open up to new perspectives for the characterization of extended  
451 peatlands with contact-less and, in general, remote geophysical methods.

452

## 453 6. Conclusions

454 Contact-less electromagnetic methods represent a valid alternative to classic ground-  
455 based geophysical methods for peat thickness detection. ~~Selected a~~ peatland located  
456 South of the Venice lagoon (Italy) ~~was selected as our study site,-;~~ we compared the  
457 results obtained by the inversion of -multi-frequency ground-based FDEM and airborne  
458 time domain EM data to data coming from direct probing and detailed high resolution  
459 ERT.]

460 The inverted results obtained from FDEM and AEM are in agreement with those  
461 obtained with the ERT detecting a resistive peat layer lying over a conductive clay  
462 substrate: the upper layer, about 1 m thick, shows a slightly larger electrical resistivity  
463 ( $> 25 \Omega \cdot m$ ) than the underlying conductive layer with lower resistivity ( $< 12 \Omega \cdot m$ ).

21

**Commented [DSSP5]:** Lines 459-460: Delete the word "Selected" in line 459 and add "as our study site" in line 460.

464 These features are in agreement with the information available on the site from shallow  
465 borehole drilling, confirming a peat thickness that varies between 80 cm and 130 cm  
466 across the selected transect, over a silty/clayey substrate.

467 Our results show that both contact-less electro-magnetic methods used in this study  
468 (FDEM and AEM) are effective in detecting the presence and electrical characteristics  
469 of peat layers over conductive substrates, potentially allowing for very fast and  
470 extended exploration surveys over large peatland sites, with a large saving of time and  
471 fieldwork if compared to traditional ground-based methods. The main difference  
472 between the two contact-less methods tested in our work lies on the accuracy in  
473 resolving the peat thickness. If the peat deposit thickness is large, the airborne AEM  
474 method can be adopted, allowing high accuracies over large territories (Silvestri et al.,  
475 2019a, 2019b). In case of thin peat deposits, FDEM provides higher vertical resolutions  
476 than AEM, substantially increasing the peat thickness mapping accuracy. We speculate  
477 that ground-based and airborne data can be used in a joint inversion scheme, with the  
478 purpose of enhancing AEM resolution where ground-based EM data are available and  
479 extend the results to larger areas where only AEM might be available in an upscaling  
480 effort: this will be the goal of near to come future studies.

481 Based on our results we conclude that the use of contact-less electro-magnetometer  
482 surveys hold the promise of becoming basic tools for peat thickness mapping, a  
483 necessary information in order to characterize these valuable natural carbon reservoirs.

484

## 485 Acknowledgements

486 This research is part of the project CReScenDo (Combining Remote Sensing  
487 Technologies for Peatland Detection and Characterization) that has received funding

**Commented [DSSP6]:** Lines 485-486: As "information" is used as a plural noun here, I suggest deleting the indefinite article "a" at the end of line 485.



488 from the European Union's Horizon 2020 research and innovation programme under  
489 the Marie Skłodowska-Curie grant agreement No. 747809.

490 AEM data are from the Flagship Project RITMARE – The Italian Research for the Sea  
491 – coordinated by the Italian National Research Council and funded by the Italian  
492 Ministry of Education, University and Research within the National Research Program  
493 2011–2013.

494 The authors declare the following competing interests: Andrea Viezzoli is the head of  
495 a small company that provides technical support for the analyses of AEM data.

496 FDEM and ERT data used for this paper are freely available through  
497 OpenAIRE/Zenodo at <http://...> with DOI: [10.5281/zenodo.3786404](https://doi.org/10.5281/zenodo.3786404).

#### 498 **References**

499 Ballhorn, U., Jubanski, J., Siebert, F., 2011. ICESat/GLAS Data as a Measurement Tool  
500 for Peatland Topography and Peat Swamp Forest Biomass in Kalimantan,  
501 Indonesia. *Remote Sens.*, 3, 1957-1982. <http://doi.org/10.3390/rs3091957>.

502 Ballhorn, U., Siebert, F., Mason, M., Limin, S., 2009. Derivation of burn scar depths  
503 and estimation of carbon emissions with LIDAR in Indonesian peatlands.  
504 *Proceedings of the National Academy of Sciences of the United States of America*,  
505 106(50), 21,213–21,218, <https://doi.org/10.1073/pnas.0906457106>.

506 Binley, A., 2015. Tools and Techniques: DC Electrical Methods, in: Schubert, G. (Ed.),  
507 *Treatise on Geophysics*, 2nd Edition, Elsevier, Vol. 11, 233-259.  
508 <http://doi.org/10.1016/B978-0-444-53802-4.00192-5>.

509 Boaga, J., Ghinassi, M., D'Alpaos, A., Deidda, G.P., Rodriguez, G., Cassiani, G., 2018.  
510 Geophysical investigations unravel the vestiges of ancient meandering channels and

511 their dynamics in tidal landscapes. *Scientific Reports*, 8:1708.  
512 <http://doi.org/10.1038/s41598-018-20061-5>.

513 Boaga, J., 2017. The use of FDEM in Hydrogeophysics, *Journal of Applied*  
514 *Geophysics*. <http://doi.org/10.1016/j.jappgeo.2017.02.011>.

515 Boaga, J., D'Alpaos, A., Cassiani, G., Marani, M., Putti, M., 2014. Plant-soil  
516 interactions in salt marsh environments: Experimental evidence from electrical  
517 resistivity tomography in the Venice Lagoon. *Geophys. Res. Lett.*, 41, 6160–6166.  
518 <http://doi.org/10.1002/2014GL060983>.

519 Boon, D., Kessler, H., Raines, M., Kuras, O., Auton, C., Williams, J., et al., 2008.  
520 Modelling Scottish peat stratigraphy using integrated electrical geophysics.  
521 [Lecture] In: Reinforced water: Engineering and environmental considerations in  
522 construction over peat, Edinburgh, Scotland, 11 March 2008.  
523 <http://nora.nerc.ac.uk/id/eprint/4830/>

524 Bourgeau-Chavez, L.L., Endres, S.L., Graham, J.A., Hribljan, J.A., Chimner, R.A.,  
525 Lillieskov, E.A., Battaglia, M.J., 2018. Mapping peatlands in boreal and tropical  
526 ecoregions, in: Liang, S. (Ed.), *Comprehensive Remote Sensing*, vol. 6. Oxford,  
527 UK: Elsevier: 24–44., pp. 24-44.

528 Carbognin, L., Tosi, L., 2003. Il Progetto ISES per l'analisi dei processi di intrusione  
529 salina e subsidenza nei territori meridionali delle Province di Padova e Venezia,  
530 Grafiche Erredici, Padova (Italy), 95 pp.

531 Cassiani, G., Bruno, V., Villa, V., Fusi, N., Binley, A.M., 2006. A saline tracer test  
532 monitored via time-lapse surface electrical resistivity tomography. *Journal of*  
533 *Applied Geophysics*, 59, 244-259, <http://doi.org/10.1016/j.jappgeo2005.10.007>.

534 Città Metropolitana Venezia: <http://webgis.cittametropolitana.ve.it/geologia>,  
535 [http://difesasuolo.provincia.venezia.it/DifesaSuolo/Index?pagina=1&id=banca\\_da](http://difesasuolo.provincia.venezia.it/DifesaSuolo/Index?pagina=1&id=banca_da)

536 ti\_idrogeologica, Banca dati geologica e idrogeologica, last access: 30 December  
537 2017.

538 Comas, X., Slater, L., 2004. Low-frequency electrical properties of peat. *Water*  
539 *Resources Research*, 40, W12414. <https://doi.org/10.1029/2004WR003534>.

540 Comas, X., Terry, N., Slater, L., Warren, M., Kolka, R., Kristiyono, A., Sudiana, N.,  
541 Nurjaman, D., Darusman, T., 2015. Imaging tropical peatlands in Indonesia using  
542 ground-penetrating radar (GPR) and electrical resistivity imaging (ERI):  
543 Implications for carbon stock estimates and peat soil characterization.  
544 *Biogeosciences*, 12(10), 2995–3007. [https://doi.org/10.5194/bg-12-2995-](https://doi.org/10.5194/bg-12-2995-2015)  
545 [2015](https://doi.org/10.5194/bg-12-2995-2015).

546 Comas, X.; Terry, N.; Hribljan, J.; Lilleskov, E. A.; Suarez, E.; Chimner, R. A.; and  
547 Kolka, R. K. 2017. Estimating belowground carbon stocks in peatlands of the  
548 Ecuadorian páramo using ground penetrating radar (GPR). *Journal of Geophysical*  
549 *Research-Biogeosciences*, 122, doi:10.1002/2016JG003550.

550 Da Lio, C., Tosi, L., Zambon, G., Vianello, A., Baldin, G., Lorenzetti, G., Manfe, G.,  
551 Teatini, P., 2013. Long-term groundwater dynamics in the coastal confined aquifers  
552 of Venice (Italy). *Estuar. Coast. Shelf Sci.*, 135, 248-259.  
553 <https://doi.org/10.1016/j.ecss.2013.10.021>.

554 de Franco, R., Biella, G., Tosi, L., Teatini, P., Lozej, A., Chiozzotto, B., Giada, M.,  
555 Rizzetto, F., Claude, C., Mayer, A., Bassan, V. and Gasparetto-Stori, G., 2009.  
556 Monitoring the saltwater intrusion by time lapse electrical resistivity tomography:  
557 The Chioggia test site (Venice Lagoon, Italy). *J. Appl. Geophys.*, 69, 117-130.  
558 <https://doi.org/10.1016/j.jappgeo.2009.08.004>.

Field Code Changed

Formatted: English (United States)

Formatted: English (United States)

559 Deidda, G.P., Díaz de Alba, P., Fenu, C, Lovicu, G., Rodriguez, G., 2019. FDEMtools:  
560 a MATLAB package for FDEM data inversion. Numerical Algorithms.  
561 <https://doi.org/10.1007/s11075-019-00843-2> (in press).

562 Deidda, G.P., Díaz de Alba, P., Rodriguez, G., 2017. Identifying the magnetic  
563 permeability in multi-frequency EM data inversion. Electron. Trans. Numer. Anal.,  
564 47,1–17. [http://doi.org/10.1553/etna\\_vol47s1](http://doi.org/10.1553/etna_vol47s1).

565 Deidda, G.P., Díaz de Alba, P., Rodriguez, G., Vignoli, G., 2020. Inversion of  
566 Multiconfiguration Complex EMI Data with Minimum Gradient Support  
567 Regularization: A Case Study. Mathematical Geosciences.  
568 <https://doi.org/10.1007/s11004-020-09855-4> (in press).

569 Deidda, G.P., Fenu, C., Rodriguez, G., 2014. Regularized solution of a nonlinear  
570 problem in electromagnetic sounding. Inverse Probl., 30 (12).  
571 <http://dx.doi.org/10.1088/0266-5611/30/12/125014>.

572 Draper, F.C., et al., 2014. The distribution and amount of carbon in the largest peatland  
573 complex in Amazonia. Environ. Res. Lett., 9. [http://doi.org/10.1088/1748-](http://doi.org/10.1088/1748-9326/9/12/124017)  
574 [9326/9/12/124017](http://doi.org/10.1088/1748-9326/9/12/124017).

575 Elijah, A.A., Folorunso, A., Olubunmi, J., 2012. An application of 2D electrical  
576 resistivity tomography in geotechnical investigations of foundation defects: A case  
577 study. Journal of Geology and Mining Research, 3(12), 142–151.  
578 <http://doi.org/10.5897/JGMR12.002>.

579 FAOSTAT 2013. FAOSTAT database. Food and Agriculture Organization of the  
580 United Nations. Available at: [http:// faostat.fao.org /](http://faostat.fao.org/)

581 Fenner, N., Freeman, C., 2011. Drought-induced carbon loss in peatlands. Nature  
582 Geoscience 4, 895–900.<http://doi.org/10.1038/ngeo1323>.

**Field Code Changed**

**Formatted:** English (United States)

**Formatted:** English (United States)

583 Gambolati, G., Putti, M., Teatini, P., Camporese, M., Ferraris, S., Gasparetto Stori, G.,  
584 Nicoletti, V., Silvestri, S., Rizzetto, F., Tosi, L., 2005. Peat land oxidation enhances  
585 subsidence in the venice watershed. EOS, TRANSACTIONS, vol. 86, p. 217-  
586 220,<http://doi.org/10.1029/2005EO230001>.

587 Gasparetto-Stori, G., Strozzi, T., Teatini, P., Tosi, L., Vianello, A., Wegmüller, U.,  
588 2012. Dem of the Veneto plain by ERS2-ENVISAT cross interferometry, in:  
589 Scappini, S., Zapparoli, S. (Eds.), 7th EUREGEO, European Congress on Regional  
590 Geoscientific Cartography and Information Systems, vol. I, Centro Stampa Regione  
591 Emilia-Romagna Publ (2012), pp. 345-350.

592 Gatti, P., Bonardi, M., Tosi, L., Rizzetto, F., Putti, M., Teatini, P., 2002. The peat  
593 deposit of the subsiding Zennare Basin, South of Venice Lagoon, Italy:  
594 geotechnical classification and preliminary mineralogical characterization, in:  
595 Camprostrini, P. (Ed.), Scientific research and safeguarding of Venice, CoRiLa  
596 Research Program 2001 Results. p. 241-258, Venezia: Corila- Istituto Veneto  
597 Scienze Lettere ed Arti, ISBN: 88-88143-12-2.

598 Holden, N.M., Connolly, J., 2011. Estimating the carbon stock of a blanket peat region  
599 using a peat depth inference model. *Catena*, 86(2), 75–85.

600 Hooijer, A., Page, S., Jauhiainen, J., Lee, W.A., Lu, X.X., Idris, A., Anshari, G., 2012.  
601 Subsidence and carbon loss in drained tropical peatlands. *Biogeosciences*, 9(3),  
602 1053-1071. <http://doi.org/10.5194/bg-9-1053-2012>.

603 Householder, J.E., Janovec, J., Tobler, M., Page, S., Lähteenoja, O., 2012. Peatlands of  
604 the Madre de Dios River of Peru: Distribution, geomorphology, and habitat  
605 diversity, *Wetlands*, 32(2), 359–368.

606 Huang, H. Won, I.J., 2003. Real-time resistivity sounding using a hand-held broadband  
607 electromagnetic sensor. *Geophysics*, 68, 1224–31.  
608 <https://doi.org/10.1190/1.1598114>.

609 Jaenicke, J., Rieley, J.O., Mott, C., Kimman, P., Siegert, F., 2008. Determination of the  
610 amount of carbon stored in Indonesian peatlands. *Geoderma*, 147, 151-158.  
611 <https://doi.org/10.1016/j.geoderma.2008.08.008>.

612 Joosten, H., 2010. The Global Peatland CO2 Picture: Peatland Status and Drainage  
613 Related Emissions in All Countries of the World. *Wetlands International*,  
614 Wageningen, Netherlands, 36 pp.

615 Keaney, A., McKinley, J., Graham, C., Robinson, M., Ruffell, A., 2013. Spatial  
616 statistics to estimate peat thickness using airborne radiometric data. *Spatial*  
617 *Statistics*, 5, 3-24. <https://doi.org/10.1016/j.spasta.2013.05.003>.

618 Kowalczyk, S., Żukowska, K. A., Mendecki, M. J., Łukasiak, D., 2017. Application of  
619 electrical resistivity imaging (ERI) for the assessment of peat properties: A case  
620 study of the Całowanie Fen, Central Poland. *Acta Geophysica*, 65(1), 223–235.  
621 <https://doi.org/10.1007/s11600-017-0018-9>.

622 McNeill, J.D., 1980. Electromagnetic terrain conductivity measurement at low  
623 induction numbers. Tech. Rep. Technical Note TN-6. Geonics Limited.

624 Nicoletti, V., Silvestri, S., Rizzetto, F., Tosi, L., Putti, M., Teatini, P., 2003. Use of  
625 remote sensing for the delineation of surface peat deposits south of the Venice  
626 Lagoon (Italy). IGARSS 2003. International Geoscience and Remote Sensing  
627 Symposium, vol. IV. Institute of Electrical and Electronics Engineers, Inc., pp.  
628 2881–2883. CD-ROM.

629 Page, S.E., Siegert, F., Rieley, J.O., Boehm, H.V., Jaya, A., Limin, S., 2002. The  
630 amount of carbon released from peat and forest fires in Indonesia during 1997.  
631 *Nature*, 420(6911), 61–65. <https://doi.org/10.1038/nature01131>.

632 Parry, L.E., West, L.J., Holden, J., Chapman, P.J., 2014. Evaluating approaches for  
633 estimating peat depth. *J. Geophys. Res. Biogeosci.*, 119, 567–576.  
634 <http://doi.org/10.1002/2013JG002411>.

635 Parsekian, A.D., Slater, L., Ntarlagiannis, D., Nolan, J., Sebesteyen, S.D., Kolka, R.K.,  
636 Hanson, P.J., 2012. Uncertainty in peat volume and soil carbon estimated using  
637 ground-penetrating radar and probing. *Soil Science Society of America Journal*,  
638 76(5), 1911–1918. <http://doi.org/10.2136/sssaj2012.0040>.

639 Rizzetto, F., Tosi, L., Carbognin, L., Bonardi, M., Teatini, P., 2003. Geomorphological  
640 setting and related hydrogeological implications of the coastal plain south of the  
641 Venice Lagoon (Italy), in *Hydrology of the Mediterranean and Semiarid Regions*,  
642 edited by E. Servat et al., IAHS Publ., 278, 463–470.

643 Silvestri, S., Christensen, C. W., Lysdahl, A.O.K., Anschütz, H., Pfaffhuber, A.A.,  
644 Viezzoli, A., 2019a. Peatland volume mapping over resistive substrates with  
645 airborne electromagnetic technology. *Geophysical Research Letters*, 46(12), 6459-  
646 6468. <https://doi.org/10.1029/2019GL083025>

647 Silvestri, S., Knight, R., Viezzoli, A., Richardson, C. J., Anshari, G. Z., Dewar, N.,  
648 Flanagan, N., Comas, X. 2019b. Quantification of Peat Thickness and Stored  
649 Carbon at the Landscape Scale in Tropical Peatlands: A Comparison of Airborne  
650 Geophysics and an Empirical Topographic Method, *J. of Geophysical Research:*  
651 *Earth Surface*, 124, pp. 1 – 17.

652 Slater, L. D., Reeve, A., 2002. Investigating peatland stratigraphy and hydrogeology  
653 using integrated electrical geophysics. *Geophysics*, 67(2), 365–378.  
654 <https://doi.org/10.1190/1.1468597>.

655 Sørensen, K. I., & Auken, E. (2004). SkyTEM – A new high - resolution helicopter  
656 transient electromagnetic system. *Exploration Geophysics*, 35(3), 191–199.

657 Teatini, P., Tosi, L., Viezzoli, A., Baradello, L., Zecchin, M., Silvestri, S., 2011.  
658 Understanding the hydrogeology of the Venice Lagoon subsurface with airborne  
659 electromagnetics. *Journal of Hydrology*, vol. 411, p. 342-354, ISSN: 0022-  
660 1694.<http://doi.org/10.1016/j.jhydrol.2011.10.017>.

661 Teatini, P., Tosi, L., Viezzoli, A., Baradello, L., Zecchin, M. and Silvestri, S., 2011.  
662 Understanding the hydrogeology of the Venice lagoon subsurface with airborne  
663 electromagnetics. *Journal of Hydrology*, 411(3-4), 342-354.  
664 <https://doi.org/10.1016/j.jhydrol.2011.10.017>.

665 Tosi, L., Carbognin, L., Teatini, P., Rosselli, R., Gasparetto Stori, G., 2000. The ISES  
666 Project subsidence monitoring of the catchment basin south of the Venice Lagoon  
667 (Italy). In: Carbognin, L., Gambolati, G., Johnson A.I., (Eds.). *Land Subsidence*,  
668 vol. II, p. 113-126, Perugia: C.N.R., Gruppo nazionale per la difesa dalle catastrofi  
669 idrogeologiche, ISBN: 88-87222-06-1.

670 Tosi, L., Teatini, P., Carbognin, L., Brancolini, G., 2009. Using high resolution data to  
671 reveal depth-dependent mechanisms that drive land subsidence: the Venice coast,  
672 Italy. *Tectonophysics*, 474, 271–284. <https://doi.org/10.1016/j.tecto.2009.02.026>.

673 Tosi, L., Teatini, P., Strozzi, T., Carbognin, L., Brancolini, G., Rizzetto, F., 2010.  
674 Ground surface dynamics in the northern Adriatic coastland over the last two  
675 decades. *Rendiconti Lincei*, 21 (Suppl. 1) (2010), pp. 115-129  
676 <https://doi.org/10.1007/s12210-010-0084-2>.



677 Tosi, L., Da Lio, C., Strozzi, T., Teatini, P., 2016. Combining L- and X-Band SAR  
678 Interferometry to Assess Ground Displacements in Heterogeneous Coastal  
679 Environments: The Po River Delta and Venice Lagoon, Italy. *Remote Sens*, 8, 308.  
680 <https://doi.org/10.3390/rs8040308>.

Field Code Changed

681 Tosi, L., Da Lio, C., Teatini, P., Menghini, A., and Viezzoli, A., 2018. Continental and  
682 marine surficial water – groundwater interactions: the case of the southern coastland  
683 of Venice (Italy), *Proc. IAHS*, 379, 387–392. [https://doi.org/10.5194/piahs-379-](https://doi.org/10.5194/piahs-379-387-2018)  
684 387-2018.

685 Turetsky, M.R., Benscoter, B., Page, S., Rein, G., van der Werf, G.R., Watts, A.e, 2015.  
686 Global vulnerability of peatlands to fire and carbon loss. *Nature Geoscience*, 8, 11-  
687 14 (2015). <http://doi.org/10.1038/NGEO2325>.

688 Van Asselen, S., Erkens, G., Stouthamer, E., Woodlerink, H. A. G., Geeraerts, R.E.E.,  
689 Hefting, M.M., 2018. The relative contribution of peat compaction and oxidation to  
690 subsidence in built-up areas in the Rhine-Meuse delta, The Netherlands. *Science of*  
691 *the Total Environment*, 636, 177– 191.  
692 <https://doi.org/10.1016/j.scitotenv.2018.04.141>.

693 Viezzoli, A., Christiansen, A.V., Auken, E., Sørensen, K.I., 2008. Quasi-3D modeling  
694 of airborne TEM data by spatially constrained inversion. *Geophysics*, 73(3), F105–  
695 F113. <https://doi.org/10.1190/1.2895521>.

Field Code Changed

696 Viezzoli, A., Tosi, L., Teatini, P., Silvestri, S., 2010. Surface water-groundwater  
697 exchange in transitional coastal environments by airborne electromagnetics: the  
698 Venice Lagoon example. *Geophys. Res. Lett.*, 37, L01402, 2010.  
699 <https://doi.org/10.1029/2009GL041572>.

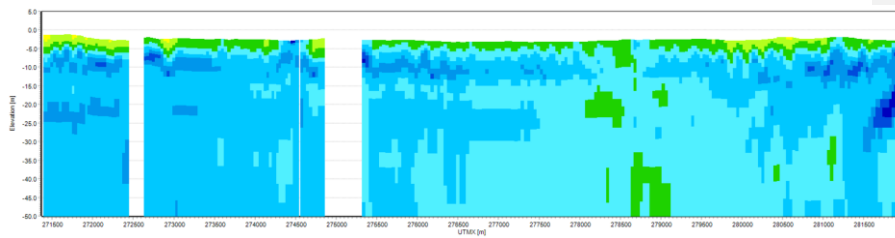
700 Walter, J., Lück, E., Heller, C., Bauriegel, A. and Zeitz, J., 2019. Relationship between  
701 electrical conductivity and water content of peat and gyttja: implications for

702 electrical surveys of drained peatlands. *Near Surface Geophysics*, 17(2), pp.169-  
703 179.

704 Zanello, F., Teatini, P., Putti, M., Gambolati, G., 2011. Long term peatland subsidence:  
705 Experimental study and modeling scenarios in the Venice coastland. *Journal of*  
706 *Geophysical Research: Earth Surface*, 116(F4).  
707 <https://doi.org/10.1029/2011JF002010>.  
708

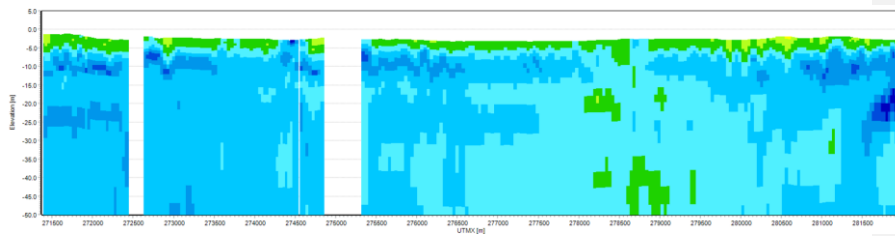
709 **Appendix**

710 a



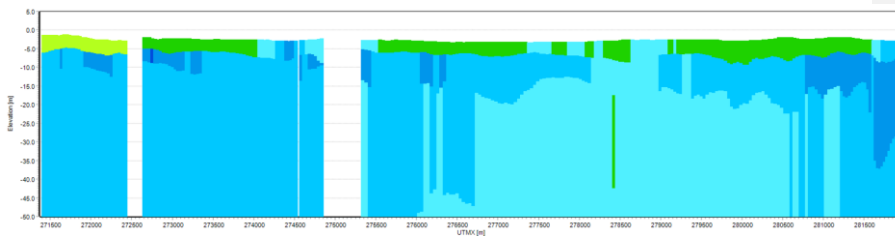
711

712 b



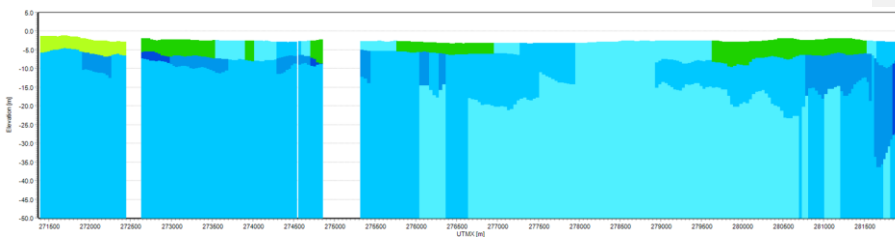
713

714 c



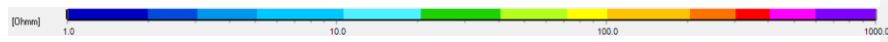
715

716 d



717

718



719 Fig. A1 – AEM resistivity model retrieved for the longest (northern) flight line using:  
720 a) 40 layers and starting with initial conductivity of  $30 \Omega \cdot \text{m}$ ; b) 40 layers and starting  
721 with initial conductivity of  $5 \Omega \cdot \text{m}$ ; c) 5 layers and starting with initial conductivity of  
722  $30 \Omega \cdot \text{m}$ ; d) 5 layers and starting with initial conductivity of  $5 \Omega \cdot \text{m}$ .